Heterogeneously integrated III–V-on-silicon multibandgap superluminescent light-emitting diode with 290 nm optical bandwidth

A. De Groote,[1,2,*] J. D. Peters,[1] M. L. Davenport,[1] M. J. R. Heck,[1] R. Baets,[2] G. Roelkens,[2] and J. E. Bowers[1]

[1]Optoelectronics Research Group, Electrical and Computer Engineering Department, University of California Santa Barbara, Santa Barbara, California 93106, USA

[2]Photonics Research Group, Department of Information Technology, Ghent University—imec, Ghent, Belgium

*Corresponding author: andreasdegroote@intec.ugent.be

Received June 3, 2014; accepted June 22, 2014;
posted July 9, 2014 (Doc. ID 213298); published August 8, 2014

A broadband superluminescent III–V-on-silicon light-emitting diode (LED) was realized. To achieve the large bandwidth, quantum well intermixing and multiple die bonding of InP on a silicon photonic waveguide circuit were combined for the first time, to the best of our knowledge. The device consists of four sections with different bandgaps, centered around 1300, 1380, 1460, and 1540 nm. The fabricated LEDs were connected on-chip in a serial way, where the light generated in the smaller bandgap sections travels through the larger bandgap sections. By balancing the pump current in the four LEDs, we achieved 292 nm of 3 dB bandwidth and an on-chip power of −8 dBm. © 2014 Optical Society of America

OCIS codes: (130.3120) Integrated optics devices; (230.3670) Light-emitting diodes; (230.5590) Quantum-well, -wire and -dot devices.
http://dx.doi.org/10.1364/OL.39.004784

While originally conceived for data and telecom applications, a broader range of applications is rapidly emerging using silicon photonics as a potential integration platform. By using standard complementary metal oxide semiconductor fabrication techniques, silicon photonic chip fabrication can achieve very high yield. However, it is difficult to realize a monolithically integrated light source on silicon due to its indirect bandgap. Therefore, III–V compounds such as InP are heterogeneously integrated on silicon-on-insulator (SOI) waveguide circuits. In these integrated devices, the gain is provided by the active region originally grown on a III–V substrate [1–3].

Superluminescent diodes (SLDs) are suitable for numerous applications, ranging from optical component testing to sensing applications, such as gyroscopes, as well as medical imaging, such as optical coherence tomography (OCT). For these applications, large bandwidth is of critical importance. For example, 300 nm of bandwidth leads to ± 3 μm of resolution in OCT. There are different approaches of extending the bandwidth of the III–V gain medium, among which are dual quantum-well (QW) design [4], multistate QWs [5], and quantum dots [6]. These structures are, however, difficult to design and optimize and operate well only using specific drive currents. Alternatively, broadband supercontinuum sources can be considered, but these typically require ultrashort pulse sources that cannot yet be integrated on the SOI waveguide circuit [7].

To address these limitations, we designed and demonstrated a superluminescent single-mode light-emitting diode (LED) with different active sections having different bandgaps, integrated on a silicon waveguide circuit. Thanks to the implantation enhanced disordering quantum well intermixing technique (IED-QWI), we can blueshift certain areas of the to-be-bonded InP die [8]. On top of that, we can bond several dies on one SOI waveguide circuit [9]. To our knowledge, this is the first time that these two techniques have been combined, although they are very complementary. With this achievement, we merged four different bandgaps in a serial manner, as indicated in Fig. 1(a).

Since two epitaxial layer stacks are bonded side by side, we have a large design freedom for the epitaxial design. Our layer stack of choice is described in Table 1. The downside of this multiple die bonding is the reduced flexibility in the positioning of the different materials. If one would use only this technique, four different dies have to be bonded next to each other. Consequently the device area grows very large. QW intermixing is a technique of changing the composition of the QWs by atom disordering. As this is lithographically defined, it does give us this extra flexibility and makes it possible to have two bandgaps in the same mesa. The maximum wavelength shift is limited to ± 125 nm around telecom wavelengths, however, as discussed later.

Because of this, our structures were designed such that each device has two mesas, each consisting of two bandgaps, as indicated in Fig. 1. The narrowest bandgap is utmost left, the largest is utmost right. This way the light can travel toward the right without suffering from strong band-to-band absorption. Any photons traveling toward the left are absorbed by the narrower bandgaps, thereby optically pumping the narrow bandgap material. In this manner, we have created a

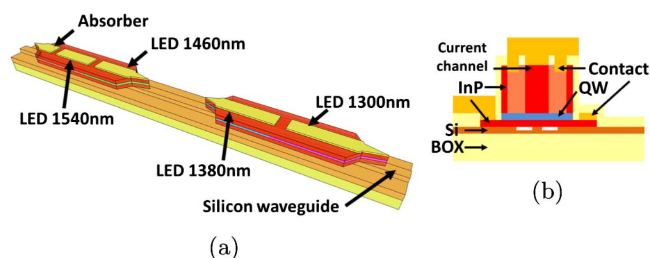

Fig. 1. Illustration of the broadband LED. (a) 3D overview. (b) Cross section of the III–V-on-silicon waveguide.

0146-9592/14/164784-04$15.00/0 © 2014 Optical Society of America

Table 1. Epitaxial Layer Stacks

No.	Layer	Thickness	Doping
9	Sacrificial InP buffer	450 nm	i
8	$In_{0.8423}GaAs_{0.3434}P$ etch stop	40 nm	i
7	n-InP bonding layer	17.5 nm	(n) 3×10^{18} cm^{-3}
6	$In_{0.85}GaAs_{0.327}P$/InP superlattice	(2×)7.5/7.5 nm	(n) 3×10^{18} cm^{-3}
5	n-InP contact	110 nm	(n) 3×10^{18} cm^{-3}
4a[a]	$In_{0.741}GaAs_{0.805}P$ well/$In_{0.9611}GaAs_{0.0025}P$ barrier	$7 \times 4.0/8 \times 8.0$ nm	i
4b[b]	$In_{0.735}GaAs_{0.845}P$ well/$In_{0.735}GaAs_{0.513}P$ barrier	$7 \times 6.5/8 \times 8.0$ nm	i
3	p-$In_{0.5305}Al_{0.4055}Ga_{0.064}As$	250 nm	(p) 10^{17} cm^{-3}
2	p-InP	1.5 μm	(p) 10^{18} cm^{-3}
1	p-$In_{0.532}GaAs$	100 nm	(p) 10^{19} cm^{-3}
0	p-InP substrate	350 μm	(p) 2×10^{18} cm^{-3}

[a]The stack with layers 4a as QWs has a PL peak at 1380 nm.
[b]The stack with layers 4b has a PL peak at 1540 nm.

one-directional device which only emits on the right side. In the design of an LED, special precautions have to be taken to prevent lasing, which would narrow the spectrum. Here, inherently it is impossible to lase for all bandgaps because the bandgap to the left will always heavily absorb the generated light, so no net roundtrip gain is possible. This is true for all bandgaps except the smallest one. Therefore, we created an extra absorbing section on the left side, by reverse biasing part of the active waveguide.

Fabrication starts with the preparation of two InP samples. First, alignment markers are etched, to be able to do an aligned bonding. To avoid delamination during bonding, they have to be lower than the bonding surface (layer 7 in Table 1), so they are etched in two steps (first a wide window in layers 8 and 9, then the actual marker in layers 6 and 7). The to-be-intermixed areas are implanted with phosphor ions into the buffer layer (9). Subsequently, they are propagated into the QWs during a 700°C/725°C thermal anneal. Because phosphor starts to evaporate at 500°C at atmospheric pressure [10], a cap layer is necessary (a SiN/SiO_2/SiN strain compensated layer). Figure 2 shows the evolution of the photoluminescence (PL) peak wavelengths (both in absolute terms and relative to each other) as a function of time for the two materials. In Fig. 2(b), one can clearly see that the maximum shift is 125 nm. At longer anneal duration, the implanted areas cease to intermix, probably because the atom gradient is no longer high enough. The QW becomes shallow and the locations of the eigenstates are hard to shift. The nonimplanted areas, on the other hand, start to shift: the thermal energy is high enough to start atom disordering without the addition of impurities. An alternative explanation would be that the growth defects start to act as the initiator of disordering. After QWI, the buffer layer is etched away, leaving a clean, flat bonding surface (layer 7). The PL spectra of the different materials are shown in Fig. 3, illustrating a broad wavelength coverage.

In the SOI sample, trenches of 250 nm depth are dry etched in the 500 nm thick silicon device layer to form the waveguide, followed by the etching of vertical outgassing channels, which increase the bonding yield. Plasma-assisted bonding is carried out as described in [11]. Note that, in this work, the SOI and InP dies have to be aligned during bonding. By using a flip chip bonder, the dies are

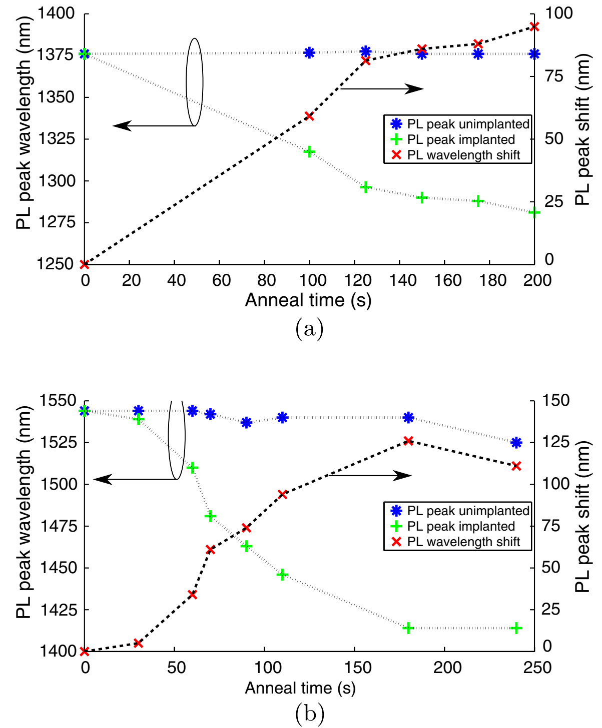

Fig. 2. Evolution of PL peak wavelength as a function of time of the different epitaxial layer stacks. (a) Epitaxial layer stack designed for 1380 nm. Anneal temperature is 700°C. (b) Epitaxial layer stack designed for 1540 nm. Anneal temperature is 725°C.

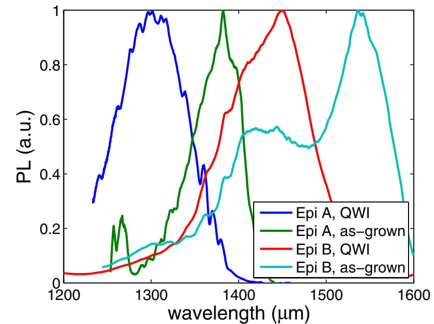

Fig. 3. Normalized PW data of two as-grown bands and shifted bandgaps. The two epitaxial layer stacks are identical except for the QWs. Those of Epi A are designed for 1380 nm, and those of Epi B for 1540 nm.

placed consecutively, with an alignment error of 2 μm. After die attachment, both dies are annealed at the same time, creating the strong covalent bonds. Because the post-bond process contains a few dry etches that might damage the silicon waveguides in between the dies, 1 μm thick SiO_2 was deposited by low-temperature plasma enhanced chemical vapor deposition. This forms a thick barrier both for the damage of dry etches as well as for preventing wet etchants to enter the waveguide trenches. After this, the InP substrates of both dies are removed, with a combination of mechanical polishing and wet etching. Because of the mechanical removal, the deposited oxide is milled away, opening the InP dies in a self-aligned manner.

The post-bond process starts with mesa definition. Reactive ion etching was used to etch down into the QW layer, and then a selective wet etch stopped on the n-InP layer. Pd/Ti/Pd/Au and Pd/Ge/Pd/Au were deposited as contact metals for the p and n contacts, respectively. The contact resistivity of these contacts was measured with the transmission line method to be $3 \times 10^{-5}\ \Omega\,\mathrm{cm}^2$ for the p contact, and $4 \times 10^{-7}\ \Omega\,\mathrm{cm}^2$ for the n contact. The mesa was 24 μm wide, so proton implantation was necessary to form a 4 μm wide current channel. Finally, the different sections are isolated from each other, by etching the p contact layer (InGaAs) and part of the p-InP. This rendered an electrical isolation of more than 50 kΩ. Note that both bonded dies are processed at the same time [12].

The tapers used to efficiently couple light from the Si/III–V hybrid structure to the passive silicon waveguide are 20 μm long and are two-staged, with a narrow p-InP layer and a gradual taper in the QWs. From [13], we know that the losses from the III–V mode to the silicon waveguide mode are of the order of 2.7 dB. Because the tapers are intermixed to transparency, the losses will be lower here compared to [13].

The length of each bandgap section is 1 mm. In this, there is a trade-off between bandwidth and efficiency, or equivalently between spontaneous and amplified spontaneous emission. In a short device, the spontaneous emission will be dominant. The total output power is then dominated by the coupling factor β (typical value of 10^{-3} [14]), which relates the power coupled to the mode to the total emitted power of spontaneous emission. In a long device, stimulated emission or gain will be of greater importance for the power, and increase the efficiency. This comes at the cost of a reduced bandwidth and longer coherence length.

Figure 4 shows the CW performance of the fabricated device at 20°C. Each section can be controlled separately, with the different p contacts being isolated by more than 50 kΩ. From the individual test structures on the chip, we know the output power of each section separately is very similar. Hence, from Fig. 4(a) we conclude that there is considerable loss in the system. The longest wavelengths have to travel farthest through the structures, and their power is lowest.

The different currents are chosen such that we have a broad, flat-top spectrum, as shown in Fig. 4(b). The pump currents were 70, 50, 300, and 140 mA for the sections at 1300, 1380, 1460, and 1540 nm, respectively. A total on-chip power of –8 dBm is achieved with a 3 dB bandwidth of 292 nm. The O, E, and S bands and part of the C band were covered, ranging from 1258 to 1550 nm.

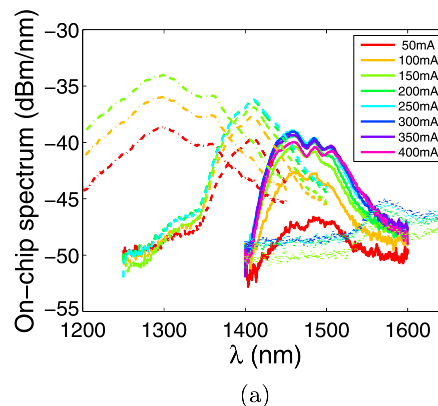

(a)

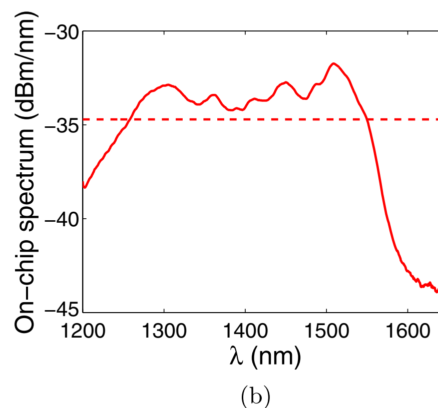

(b)

Fig. 4. On-chip spectra of the depicted device. (a) Different sections pumped separately. We used dashed, dashed–dotted, solid, and dotted lines for the sections at 1300, 1380, 1460, and 1540 nm, respectively. (b) Balanced pumping to optimize the 3 dB bandwidth. The pumping currents were 70, 50, 300, and 140 mA for the sections at 1300, 1380, 1460, and 1540 nm, respectively.

It can be concluded that the loss, which was observed in Fig. 4(a), is mainly due to residual absorption in the QWs the light has to travel through. When all sections are pumped, the difference in power is nearly gone.

From the dotted line in Fig. 4(a), one may conclude that section emits at 1580 nm rather than 1540 nm. This is contradicted by our measurement of the backside emission of the absorbing section (when forward biasing it), which does show a maximum at 1540 nm (not shown here). Also here the residual absorption is to blame. Since this absorption is below-bandgap absorption, it is highly dependent on the wavelength. The shorter wavelengths are much more absorbed than the longer ones. Light is generated with a maximum around 1540 nm, but the shorter wavelengths are absorbed. Since we measure the product of both emission and absorption the measured maximum is 1580 nm rather than 1540 nm. A similar behavior is seen in Fig. 4(b), where the maximum at 1500 nm is highly dependent on the pumping conditions of both sections. Instead of absorption, there is below-bandgap gain. This highly asymmetric gain profile amplifies the shorter wavelengths much more than the

longer, causing the maximum to shift to 1500 nm rather than 1540 nm.

Even with this loss factor, the total emitted power is not as high as can be expected (order of milliwatt). We believe that this can be attributed to fabrication imperfections. Because the p contact was not ohmic on one of the dies, we had to locally anneal it by a burn-in of 1750 mA, ramped in steps of 30 mA each 2 s. This might lead to nonuniform contact resistance along the length of the gain medium. Consequently, part of the QWs might not be pumped as strongly and absorb, leading to an overall decrease in gain.

For the first time, to our knowledge, QWI and multiple die bonding were combined. In this manner, we have realized a broadband, single-mode LED coupled to a silicon waveguide. Four different bandgaps were created and merged in order to cover the O, E, S, and C bands. The device was designed to be one directional by arranging the bandgaps from narrow to wide. When pumping the different sections to achieve a flat-top spectrum, we managed to achieve 292 nm 3 dB bandwidth, while the total power was −8 dBm.

This research was supported by DARPA MTO under the EPHI contract and the FP7-ERC-InSpectra project. Andreas De Groote thanks the Research Foundation Flanders (FWO) for a research grant and also the Belgian American Educational Foundation (BAEF) for the support.

References

1. S. Keyvaninia, S. Verstuyft, L. Van Landschoot, D. Van Thourhout, G. Roelkens, G. Duan, F. Lelarge, J. Fedeli, S. Messaoudene, T. De Vries, B. Smalbrugge, E. Geluk, J. Bolk, and M. Smit, Opt. Lett. **38**, 5434 (2013).
2. M. Heck, J. F. Bauters, M. L. Davenport, J. K. Doylend, S. Jain, G. Kurczveil, S. Srinivasan, Y. Tang, and J. E. Bowers, IEEE J. Sel. Top. Quantum Electron. **19**, 6100117 (2013).
3. G. Roelkens, L. Liu, D. Liang, R. Jones, A. Fang, B. Koch, and J. Bowers, Laser Photon. Rev. **4**, 751 (2010).
4. B.-R. Wu, C.-F. Lin, L.-W. Laih, and T.-T. Shih, Electron. Lett. **36**, 2093 (2000).
5. J. Song, S. Cho, I. Han, Y. Hu, P. Heim, F. Johnson, D. Stone, and M. Dagenais, IEEE Photon. Technol. Lett. **12**, 783 (2000).
6. A. Kovsh, A. Gubenko, I. Krestnikov, D. Livshits, S. Mikhrin, J. Weimert, L. West, G. Wojcik, D. Yin, C. Bornholdt, N. Grote, M. Maximov, and A. Zhukov, Proc. SPIE **6996**, 69960V (2008).
7. J. Safioui, F. Leo, B. Kuyken, S.-P. Gorza, S. K. Selvaraja, R. Baets, P. Emplit, G. Roelkens, and S. Massar, Opt. Express **22**, 3089 (2014).
8. S. R. Jain, Y. Tang, H.-W. Chen, M. N. Sysak, and J. E. Bowers, J. Lightwave Technol. **30**, 671 (2012).
9. H.-H. Chang, A. W. Fang, M. N. Sysak, H. Park, R. Jones, O. Cohen, O. Raday, M. J. Paniccia, and J. E. Bowers, Opt. Express **15**, 11466 (2007).
10. F. Riesz, L. Dobos, C. Vignali, and C. Pelosi, Mater. Sci. Eng. B **80**, 54 (2001).
11. D. Liang and J. Bowers, J. Vac. Sci. Technol. B **26**, 1560 (2008).
12. C. Zhang, S. Srinivasan, Y. Tang, M. J. Heck, M. L. Davenport, and J. E. Bowers, Opt. Express **22**, 10202 (2014).
13. M. Davenport, M. Heck, and J. E. Bowers, in *Conference on Lasers and Electro-Optics*, *Quantum Electronics and Laser Science*, *Fundamental Science* (Optical Society of America, 2013), paper JTu4A.25.
14. J. Park and X. Li, J. Lightwave Technol. **24**, 2473 (2006).